This article was downloaded by: *[Ecole Centrale Paris]*
On: *27 January 2009*
Access details: *Access Details: [subscription number 790383386]*
Publisher *Taylor & Francis*
Informa Ltd Registered in England and Wales Registered Number: 1072954 Registered office: Mortimer House, 37-41 Mortimer Street, London W1T 3JH, UK

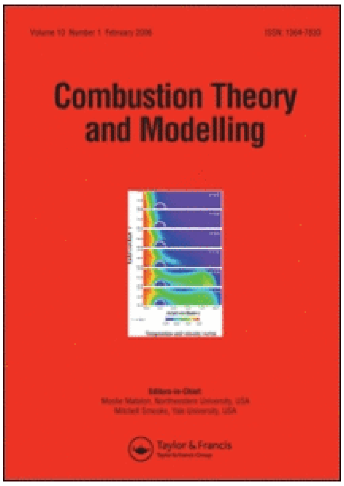

Combustion Theory and Modelling
Publication details, including instructions for authors and subscription information:
http://www.informaworld.com/smpp/title~content=t713665226

Mass transfer and combustion in transcritical non-premixed counterflows

L. Pons [a]; N. Darabiha [a]; S. Candel [ab]; G. Ribert [c]; V. Yang [d]
[a] Laboratoire EM2C, CNRS, Ecole Centrale Paris, Châtenay, Malabry, France [b] Institut Universitaire de France, [c] Laboratoire CORIA, CNRS, Université de Rouen, Saint Etienne du Rouvray, France [d] The Pennsylvania State University, University Park, PA, USA

Online Publication Date: 01 February 2009

To cite this Article Pons, L., Darabiha, N., Candel, S., Ribert, G. and Yang, V.(2009)'Mass transfer and combustion in transcritical non-premixed counterflows',Combustion Theory and Modelling,13:1,57 — 81

To link to this Article: DOI: 10.1080/13647830802368821

URL: http://dx.doi.org/10.1080/13647830802368821

PLEASE SCROLL DOWN FOR ARTICLE

Full terms and conditions of use: http://www.informaworld.com/terms-and-conditions-of-access.pdf

This article may be used for research, teaching and private study purposes. Any substantial or systematic reproduction, re-distribution, re-selling, loan or sub-licensing, systematic supply or distribution in any form to anyone is expressly forbidden.

The publisher does not give any warranty express or implied or make any representation that the contents will be complete or accurate or up to date. The accuracy of any instructions, formulae and drug doses should be independently verified with primary sources. The publisher shall not be liable for any loss, actions, claims, proceedings, demand or costs or damages whatsoever or howsoever caused arising directly or indirectly in connection with or arising out of the use of this material.

Combustion Theory and Modelling
Vol. 13, No. 1, 2009, 57–81

Mass transfer and combustion in transcritical non-premixed counterflows

L. Pons,[1,*] N. Darabiha,[1] S. Candel,[1,2] G. Ribert[3] and V. Yang[4]

[1]*Laboratoire EM2C, CNRS, Ecole Centrale Paris, 92295 Châtenay-Malabry, France;* [2]*Institut Universitaire de France;* [3]*Laboratoire CORIA, CNRS, Université de Rouen, 76801 Saint Etienne du Rouvray, France;* [4]*The Pennsylvania State University, University Park, PA 16802, USA*

(*Received 19 December 2007; final version received 7 June 2008*)

The problem of transcritical mass transfer and combustion is considered in the counterflow geometry established at ambient pressures exceeding the critical pressure of the fluids but for an injection temperature (or injection temperatures) below critical. Real gas effects taking place under these conditions are treated with suitable models for thermodynamics and transport properties. A set of routines designated as ‘TransChem’ is constructed to extend the standard ‘Chemkin’ package to the transcritical regime. Three configurations are investigated. In the first case a low temperature oxygen stream impinges on a high temperature supercritical stream of the same substance and the ambient pressure exceeds the critical pressure. The structure of this flow is determined numerically and the mass transfer taking place between the dense oxygen and the hot stream is evaluated. It is shown that this rate can be correlated in terms of a transfer number which depends on the hot and cold temperatures and on the critical temperature. The mass transfer rate is also found to evolve like the square root of the strain rate. In the second case a flame is formed in the counterflow of a stream of cold oxygen injected at a temperature which is below critical and impinges on a supercritical stream of methane. In this flow, the flame is established in the light gas region adjacent to a sharp density gradient. The flame structure is close to that found in a gaseous situation except for the very large density change on the oxygen side which fixes the oxygen mass transfer rate to the flame. In the third case, the two streams are transcritical with temperatures below the respective critical values. The flow features two sharp gradients on the oxygen and methane sides and the flame is established between these two layers in the low density gaseous region.

Keywords: transcritical; high pressure; mass transfer; strained flames

1. Introduction

Many practical systems like gas turbines, aero and automotive engines operate at elevated pressures. In many cases one of the reactants is injected in a liquid form at a temperature which is below the critical value but at a pressure which exceeds the critical pressure. This type of transcritical injection prevails in the case of cryogenic rocket engines, which motivates the present investigation. The pressure takes values which are typically of the order of 10 MPa but may reach levels as high as 40 MPa. Propellants, usually oxygen, hydrogen or methane, are injected in a transcritical or supercritical state. The analysis of combustion under such extreme conditions has progressed substantially during the

---

[*] Corresponding author. Email: laetitia.pons@em2c.ecp.fr

ISSN: 1364-7830 print / 1741-3559 online

DOI: 10.1080/13647830802368821
http://www.tandf.co.uk/journals

recent period. On the experimental level, hot fire tests carried out in model scale facilities have provided considerable information on the combustion process. This is exemplified in Juniper *et al.* [1] who describe the structure of high pressure liquid oxygen/gaseous hydrogen (LOx/GH$_2$) jet flames formed by coaxial injection and by Singla *et al.* [2] who consider combustion of transcritical oxygen with supercritical or transcritical methane. It is found in particular that coaxial injection of two transcritical reactants produces an unusual flame structure comprising two conical regions of light emission indicating that chemical conversion takes place in two separate but embedded layers of reaction. One reactive layer develops in the near vicinity of the oxygen jet boundary while the other spreads near the outer methane boundary. The structure of flames formed by two transcritical propellants clearly differs from those observed in more standard conditions.

The problem of transcritical combustion is also considered in many recent numerical simulations of high pressure flames. These calculations reflect the real gas behaviour of supercritical fluids. For example, Harstad *et al.* [3] propose an improved equation of state for supercritical fluids. Direct numerical simulations of mixing layers under high pressure and temperature are carried out in [4]. Large eddy simulations of transcritical reactants are reported by Oefelein and Yang [5] and Zong *et al.* [6] in a coaxial configuration. A number of studies have also focused on spherical droplets of transcritical fluids placed in a supercritical environment, see [7]. The spherical geometry is a useful model because the corresponding problem is essentially one dimensional simplifying the analysis. It is known however from experiments that the atomization process which governs subcritical injection of liquids and gives rise to a spray of droplets is not operative under transcritical conditions. Experiments do not show droplets but a highly wrinkled frontier separating the dense transcritical propellant from the surrounding lighter fluid. Mass transfer takes place from this dense jet and is essentially governed by the amount of exchange surface area and the local turbulent state of the flow. This can be described in terms of the local strain rate or scalar dissipation. Under such circumstances it has become standard to represent the local flame elements in terms of strained flames. The turbulent flame is then viewed as a collection of strained reactive layers which are convected and distorted by the flow but can be identified. The strained flame geometry considered in this article is then directly useful to the modelling of transcritical flames.

Much of the work on high pressure non-premixed counterflow flames considers reactants fed at a temperature which exceeds the critical value and at intermediate levels of pressure [8]. The flame structure is in that case not so different from that found under lower pressure injection conditions. A major issue in these studies is that of the pressure exponent. It is shown for example that the reaction rate per unit flame surface scales like $p^{1/2}$ and that the flame thickness decreases with pressure like $p^{-1/2}$ [9]. Injection under low temperature conditions corresponding to a trancritical state of the fluid is less well documented. A recent article [10] deals with the structure of high pressure liquid oxygen/gaseous hydrogen counterflow flames. Oxygen is injected at low temperature and the flame structure is determined by making use of a real gas equation of state and thermodynamics and modified transport coefficients reflecting real gas effects. The present article complements this effort in various directions. The objectives are (1) to develop methods for dealing with real gas effects under transcritical conditions and (2) to use these general tools to study generic mass transfer and combustion problems to understand the physics of transcritical flames. The counterflow geometry is considered at a pressure exceeding the critical values of both reactants, to examine three modelling problems. In the first, low temperature transcritical oxygen is injected against a high temperature stream of the same fluid. The objective in this case is to determine the mass transfer of oxygen from the dense region to the light gas. The second problem deals with the structure of non-premixed flames formed by a stream of low temperature transcritical oxygen impinging on a stream of supercrtical methane (injection temperature of methane is above its critical value). In the third problem, the transcritical oxygen stream is opposed to a transcritical stream of methane. In that case the two reactants are injected at low temperature but high pressure.

At this point it is worth recalling that strained flame configurations of the type used in this investigation are considered in many previous studies of turbulent gaseous flames because they allow a suitable description of the local flame elements. These flamelet structures are used to estimate the local rates of reaction per unit flame surface or to obtain the mass transfer from the dense stream when this stream is injected in a transcritical state. This approach has been exploited for example in [11] to develop a turbulent combustion model for transcritical cryogenic jet flames but strained flames are used in many other turbulent combustion modelling investigations. One important aspect of this geometry is that it reflects the local level of scalar dissipation (a quantity which can be linked to the strain rate). This article begins with a detailed account of the treatment of real gas effects of transcritical fluids (Section 2). Equation of state, thermodynamics and transport coefficient modelling are considered successively. A new set of computational routines is developed to extend the Chemkin package to the transcritical domain. This augmented version designated as TransChem is described in this section. The balance equations representing counterflow flames are considered in Section 3. These equations must be modified to account for real gas effects. It is shown in that section that it is simpler to use a balance of enthalpy instead of the more common temperature equation employed for perfect gases. Both types of equations provide exactly equivalent results in the perfect gas case but the enthalpy form remains essentially the same when there are real gas effects. Modifications of the balance equations to include real gas effects and corresponding mixing rules are briefly reviewed in Section 3. Results of simulations for the three problems considered in this study are discussed in Section 4.

2. Thermodynamics and transport properties of transcritical fluids

In transcritical combustion where pure oxygen is used as oxidizer, reactants may be injected at cryogenic temperatures of about 80 K, and the flame temperature reaches values in excess of 3000 K. The temperature range is quite large and it is essential to predict the fluid behaviour over this whole range and for a wide interval of pressures. It is first important to derive a suitable thermodynamic representation of transcritical behaviour. This issue is extensively discussed in the recent literature and results obtained provide useful guidelines. Systematic tests of equations of state carried out for pure oxygen, hydrogen and methane indicate that cubic equations constitute the best compromise between calculation cost and precision. It is concluded from these tests that the modified Peng–Robinson equation [3] provides an accurate representation of the thermodynamical state of pure species like O_2, CH_4 and H_2 and that this equation can be used in conjunction with mixing rules to describe complex mixtures over the ranges of temperature and pressure of interest.

For a pure substance, the Peng–Robinson equation of state takes the form

$$p = \frac{RT}{V-b} - \frac{a(T)}{V(V+b)+b(V-b)} \tag{1}$$

where R is the perfect gas constant, T is the temperature, V is the molar volume, $a(T)$ and b are the Peng–Robinson coefficients defined in (2) and (3) respectively.

$$a(T) = 0.45724\frac{R^2T_\mathrm{c}^2}{p_\mathrm{c}}\alpha(T) \tag{2}$$

$$b = 0.0778 \frac{RT_c}{p_c} \tag{3}$$

where T_c and p_c are respectively the critical temperature and pressure of the considered species and $\alpha(T)$ is defined by:

$$\alpha(T) = \left(1 + m\left[1 - (T/T_c)^{1/2}\right]\right)^2 \tag{4}$$

where m is given in terms of the acentric factor ω which takes into account the polarity of the species under consideration

$$m = 0.37464 + 1.54226\omega - 0.26992\omega^2 \tag{5}$$

Mixtures of different species are described by mixing rules. The coefficients appearing in the equation of state are determined according to the following expressions:

$$a_m = \sum_{i=1}^{N} \sum_{j=1}^{N} X_i X_j a_{ij}, \quad b_m = \sum_{i=1}^{N} X_i b_i \tag{6}$$

where N is the number of species in the mixture and X_i is the molar fraction of the i-th species in the mixture. The cross term a_{ij} is given by:

$$a_{ij} = (a_i a_j)^{1/2}(1 - k_{ij}) \tag{7}$$

where k_{ij} is the binary interaction factor which takes into account the interaction between the i-th and j-th species. This empirical parameter is determined experimentally. It is approximately equal to zero for hydrocarbon–hydrocarbon pairs and never exceeds 0.15 for the few available experimental data [12]. This factor is often taken equal to zero for simplicity an assumption which is also used in what follows. The coefficients a_i are given by:

$$a_i = 0.45724 \frac{R^2 T_{c,i}^2}{p_{c,i}} \left[1 + m_i \left(1 - (T/T_{c,i})^{1/2}\right)\right] \tag{8}$$

where $T_{c,i}$ and $p_{c,i}$ designate the critical temperature and pressure of the i-th species. In the previous expression b_i is given by:

$$b_i = 0.0778 \frac{RT_{c,i}}{p_{c,i}} \tag{9}$$

The critical properties of reactants considered in liquid rocket propulsion are gathered in Table 1. Thermodynamic properties are conveniently determined with the departure

Table 1. Critical properties of reactants: oxygen, methane and hydrogen.

	p_c [Mpa]	T_c [K]	ρ_c [kg·m^{-3}]
O_2	5.043	154.581	436.1
CH_4	4.599	190.564	162.6
H_2	1.315	33.19	30.12

function method [3]. This consists in first calculating thermodynamic properties in a standard state. A typical thermodynamic variable F is determined by correcting the standard state contribution to account for real gas effects represented by the Peng–Robinson equation of state. The departure function F_{PR} corresponds to the deviation of the real gas with respect to a reference perfect gas. Standard state enthalpy and entropy expressions are developed in [3] with coefficients fitted for the temperature range and species under consideration.

$$F = F_{\mathrm{PR}} + F^0 \tag{10}$$

Thermodynamic functions like molar enthalpy H, molar internal energy E or molar specific heat C_p, can be expressed with this method

$$H = \left[\int_{\infty}^{v}\left(T\left(\frac{\partial p}{\partial T}\right)_v - p\right)dv + RT(Z-1)\right] + H^0 \tag{11}$$

$$E = \left[\int_{\infty}^{v}\left(T\left(\frac{\partial p}{\partial T}\right)_v - p\right)dv\right] + E^0 \tag{12}$$

$$C_p = \left[\int_{\infty}^{v} T\left(\frac{\partial^2 p}{\partial T^2}\right)_v dv - T\left(\frac{\partial p}{\partial T}\right)_v^2 \Bigg/ \frac{\partial p}{\partial v} - R\right] + C_p^0 \tag{13}$$

where the superscript 0 denotes the thermodynamic function taken in a reference state and Z represents the compressibility factor (Equation 14).

$$Z = \frac{pv}{RT} \tag{14}$$

Exact expressions of thermodynamic properties calculated with the Peng–Robinson equation of state are gathered in Appendix A.

Typical results of the previous description are plotted in Figure 1(a) and 1(b) which provide the density of oxygen and methane over a wide range of temperatures including

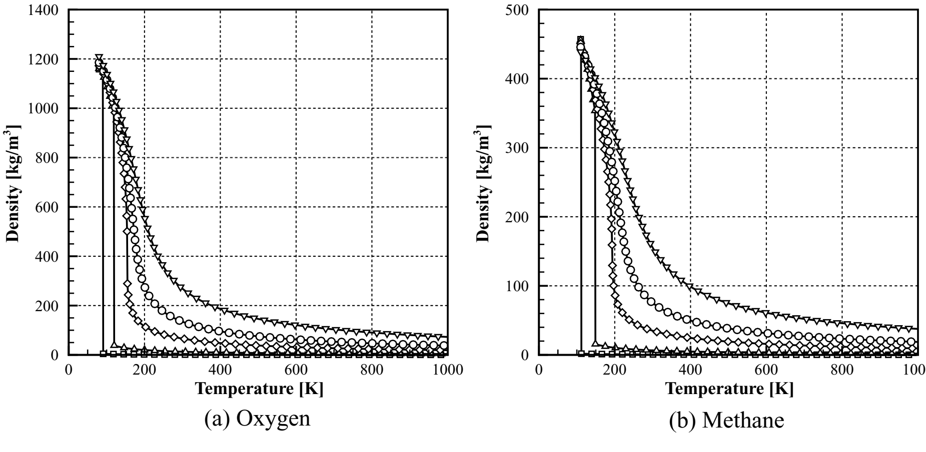

(a) Oxygen

(b) Methane

Figure 1. Evolution of the density of reactants over a range of temperatures including transcritical and supercritical states for different ambient pressures: 0.1 MPa (□), 1 MPa (△), 5 MPa (◇), 10 MPa (○), and 20 MPa (△). (a) oxygen, (b) methane.

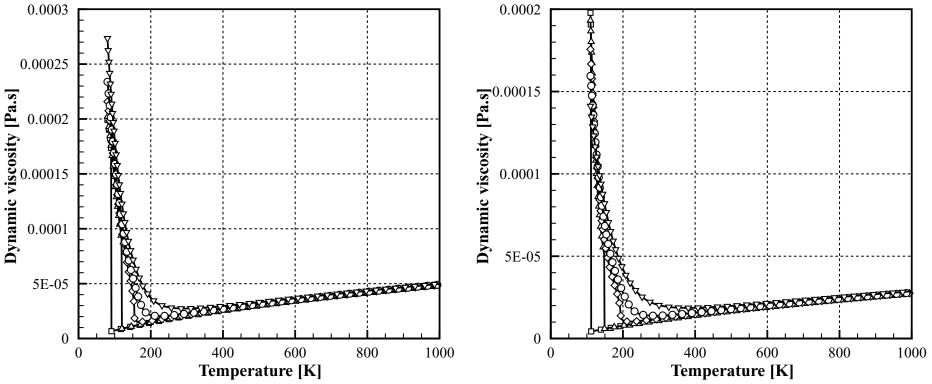

(a) Oxygen (b) Methane

Figure 2. Evolution of the dynamic viscosity of reactants over a range of temperatures including transcritical and supercritical states for different ambient pressures: 0.1 MPa(□), 1 MPa (△), 5 MPa (◇), 10 MPa (○), and 20 MPa (▽). (a) oxygen, (b) methane.

liquid, transcritical and supercritical (gaseous) states for pressures from 0.1–20 MPa. The changes in state are clearly visible when the pressure is below critical. In that case there is a discontinuity in the density evolution. The continuous transition from the transcritical to the supercritical state at pressures above critical is also well represented. Results of calculations are close to NIST [13] data and in most of the range the relative error is less than 1%. The equation of state is therefore quite suitable at low and high pressure and for a wide range of temperatures.

Transport coefficient anomalies related to real gas behaviour are reviewed by Congiunti *et al.* [14]. Transport models for high pressure fluids are generally based on the Chapman–Enskog theory (CET) or on the corresponding state theory (CST). Viscosity of transcritical fluids is suitably represented by the model derived by Chung *et al.* [15]. The model is based on the Chapman–Enskog theory, formulated for dilute gases with an added correction taking into account real gas effects at high pressure. The dynamic viscosity can be expressed by $\mu = \mu^0\mu^*$ where μ^0 is the low pressure viscosity and μ^* is the high pressure correction term. Results obtained with this model for oxygen and methane are displayed in Figure 2. The model assures a continuous transition between subcritical and transcritical conditions. When the pressure exceeds the critical value, the viscosity coefficient behaves like that of a gas when the temperature is superior to the critical temperature ($T > T_c$) and follows the standard evolution for a liquid when this temperature falls below the critical value ($T < T_c$). Transition between these two limiting cases is smoothly described by the model. The calculated values of viscosity are in excellent agreement with NIST [13] data for the range of pressures of interest (0.1–20 MPa) as shown in Appendix B.

According to [14] the thermal conductivity of a high pressure fluid is best predicted by the Ely and Hanley model [16, 17] which relies on an extension of the corresponding states theory (CST). The thermal conductivity is represented by summing two contributions $\lambda = \lambda' + \lambda''$. The first, λ', arises from the transfer of energy from collisional or translational effects and the other, λ'' describes the transfer of energy through the internal degrees of freedom. Figure 3 shows typical results of calculation of the thermal conductivity of oxygen and methane over a range of temperatures covering both subcritical and transcritical conditions and for pressures of 0.1–20 MPa. The changes of state are clearly visible when the pressure is below critical with a discontinuity in the transport coefficient. A continuous

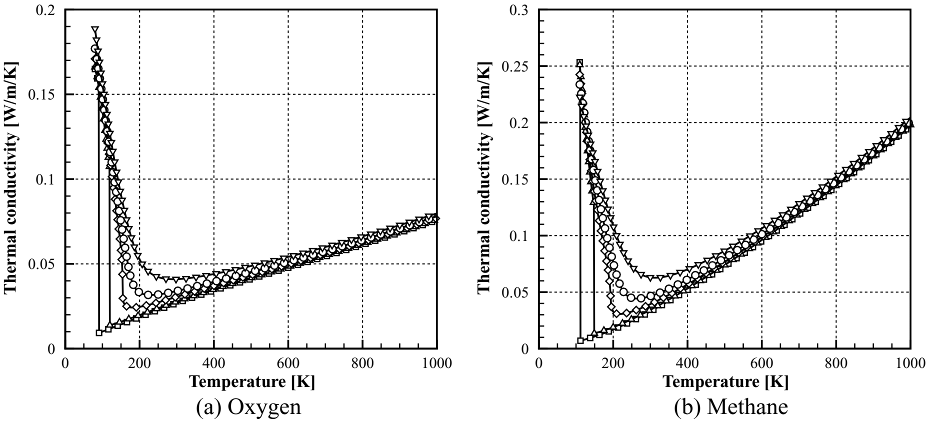

Figure 3. Evolution of the thermal conductivity of reactants over a range of temperatures including transcritical and supercritical states for different ambient pressures: 0.1 MPa(□), 1 MPa (△), 5 MPa (◇), 10 MPa (○), and 20 MPa (∇). (a) oxygen, (b) methane.

passage from the transcritical state to the supercritical state for pressures above critical is also very well represented. Agreement with NIST data is quite good (see Appendix B). The modelling of the binary mass diffusivity coefficients constitutes a challenge because the available experimental data are scarce. Harstad and Bellan [18] propose estimates of these coefficients from a corresponding states theory and expressions based on kinetic theory and experimental data correlations. However, the data are only available for a limited number of species pairs. Since combustion applications involve a large number of species one may use an alternative approach relying on a scheme similar to that used to model viscosity. The binary diffusion coefficients are first estimated for low values of pressure. The corresponding estimates D^0_{ij} are computed using the standard model of the Transport library [19]. High pressure effects are then included by applying corrections devised by Takahashi [20] $D_{ij} = D^0_{ij} f(\theta_R, \pi_R)$ where θ_R and π_R respectively represent temperature and pressure normalized by the critical values.

The previous expressions provide a unified treatment for the description of the thermodynamic state and transport properties of transcritical fluids. The corresponding models were coded in a specific set of routines designated as TransChem describing real gas behaviour for pure species or mixtures over wide ranges of pressure and temperature. This library provides the high pressure thermodynamic variables and transport models described earlier. The structure of TransChem is given in Figure 4. TransChem uses the Chemkin packages [21, 19] to determine properties in the standard state where the fluid behaves like a perfect gas. As a consequence, the standard state properties adopted in the present analysis are consistent with those used in perfect gas calculations but differ to some extent from those derived in [3]. The present choice has the advantage to exactly follow standard methods when ideal gas conditions are fulfilled. A typical variable calculated with the departure function methodology $F = F_{PR} + F^0$ essentially coincides with F^0 (calculated with standard Chemkin routines) in the limiting case where the gas is nearly ideal and the departure function F_{PR} vanishes. Additional details on the modelling of thermodynamic functions and transport properties are given in Appendix A. Chemical kinetics is handled with standard Chemkin.

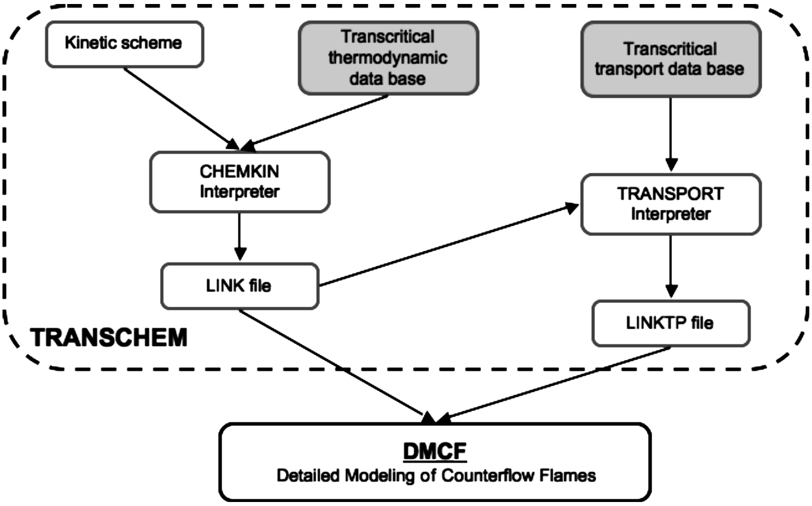

Figure 4. The transcritical fluid library TransChem and its insertion in the flame code.

3. Flow modelling under transcritical conditions

The modelling of transcritical flows poses a challenge because thermodynamic functions and transport properties depart from perfect gas behaviour as discussed in the previous section. Balance equations and if necessary, numerical methods have to be modified to take into account these phenomena. These problems are tackled by Meng and Yang [22] with a unified treatment of general fluid thermodynamics and transport in combination with a preconditionning technique. In standard approaches of counterflow flame modelling, the energy balance equation is formulated in terms of temperature as exemplified in [23] or [24]. This formulation can be derived from the total energy balance equation and from the ideal gas law since $dh = c_p dT$.

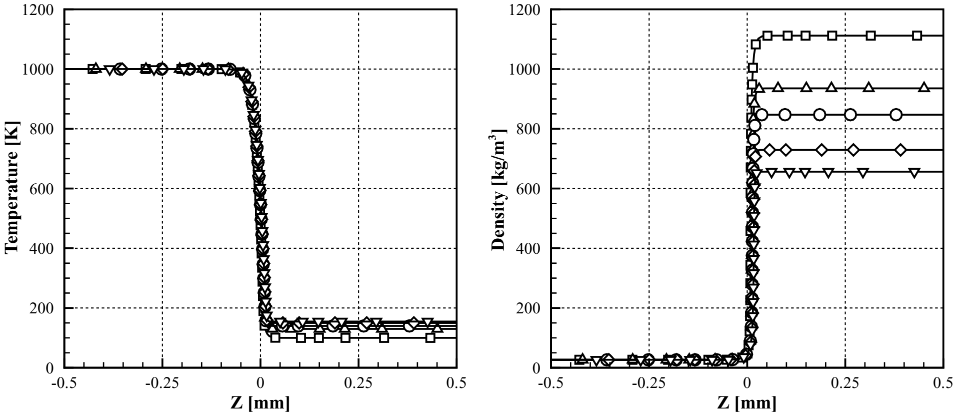

(a) Temperature profiles (b) Density profiles

Figure 5. Temperature and density profiles in a counterflow formed by a stream of transcritical oxygen impinging on a stream of supercritical oxygen. Profiles correspond to different injection temperatures of the cold fluid: $T_c = 154.581$ K (∇), 150 K ($\diamond$), 140 K ($\circ$), 130 K ($\triangle$), 100 K ($\square$). The ambient pressure is fixed at 7 MPa and the strain rate at $\epsilon_s = 1000$ s^{-1}.

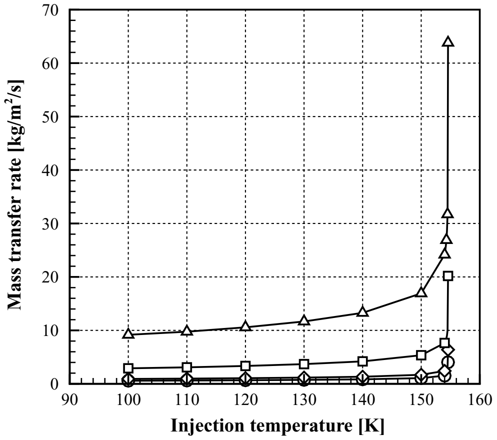

Figure 6. Mass transfer rate plotted as a function of injection temperatures of the transcritical oxygen for different values of the strain rate: 40 s^{-1} (○), 100 s^{-1} (□), 1000 s^{-1} (◇), 10 000 s^{-1} (∇). The ambient pressure is fixed at 7 MPa.

When considering real gases, the problem becomes more complex as the enthalpy differential is also a function of pressure and species differentials. This quantity given for example by Meng and Yang [22], can be expressed as a function of pressure p, temperature T, and the N mass fractions $(Y_i)_{i=1,N}$:

$$dh = B_T dT + B_p dp + \sum_{i=1}^{N} B_{Y_i} dY_i \tag{15}$$

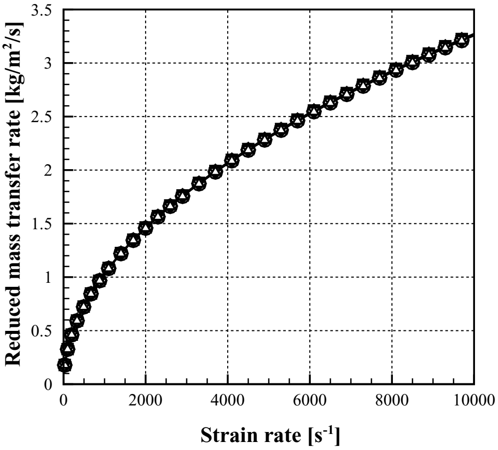

Figure 7. Reduced mass transfer rate obtained by dividing $\dot{m}_v$ by the correlation function $g(B_T)$ defined by (23). This quantity is plotted as a function of the strain rate for different injection temperatures of the transcritical flow: 110 K (○), 120 K (◇), 130 K (∇), 140 (△). The ambient pressure is fixed at 7 MPa.

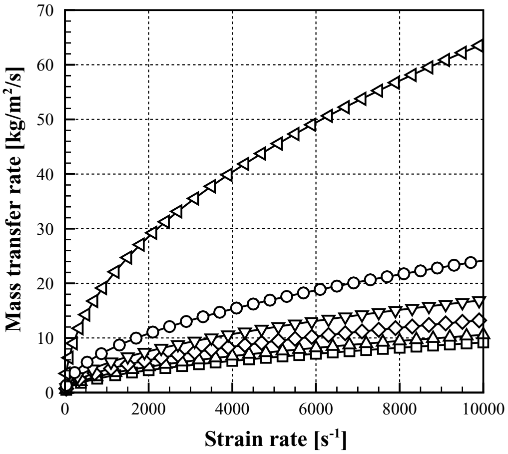

Figure 8. Evolution of the mass transfer rate with the strain rate for different injection temperatures of the transcritical oxygen stream: $T_c = 154.581$ K (◁), 154 K (○), 150 K (▽), 140 K (◇),120 K (△), 100 K (□). The ambient pressure is fixed at 7 MPa.

where:

$$B_T = c_v - \frac{1}{\rho}\left(\frac{\partial p}{\partial T}\right)_{\rho_i}\left(\frac{\partial \rho}{\partial T}\right)_{T,Y_i}\left(\sum_{i=1}^{N} Y_i\tilde{e}_i - e - \frac{p}{\rho}\right)$$

$$B_p = \frac{1}{\rho} + \frac{1}{\rho}\left(\frac{\partial \rho}{\partial p}\right)_{T,Y_i}\left(\sum_{i=1}^{N} Y_i\tilde{e}_i - e - \frac{p}{\rho}\right)$$

$$B_{Y_i} = \tilde{e}_i - \left(\frac{\partial \rho}{\partial p}\right)_{T,Y_i}\left(\sum_{i=1}^{N} Y_i\left(\frac{\partial \rho e}{\partial \rho_i}\right)_{T,\rho_{j\neq i}} - e - \frac{p}{\rho}\right)\left(\frac{\partial p}{\partial \rho_i}\right)_{T,\rho_{j\neq i}}$$

where $\tilde{e}_i$, the partial-density internal energies corresponding to the i-th species, is defined by $(\partial\rho e/\partial\rho_i)_{T,\rho_{j\neq i}}$ for each of the N species considered in the study. These expressions are equivalent to those found in [22] but the summation is now carried out from 1 to N instead of 1 to $N-1$ adopted in [22] to reduce the number of species equations by one.

Using these expressions, it is possible to treat the energy balance equation in terms of temperature by making use of Equation (15), but because of real gas effects there are many additional terms. One also has to calculate c_v, the internal and partial internal energies and the partial enthalpies in the real gas approach. Expressions of thermodynamic functions required are given in Appendix A and are fairly complex and the corresponding computational cost required to calculate these properties is augmented. The treatment proposed in the present article follows a different path. The complexities of the temperature equation are avoided by making use of the enthalpy formulation of the energy equation. In this way, the real gas thermodynamics only appears in the determination of the mixture enthalpy h, and of the species enthalpies, h_k $(k = 1, N)$. This alternative formulation has been first validated by showing that it is exactly equivalent to the standard description used to calculate counterflow flames of perfect gases. Solutions obtained with the temperature form of the energy equation and those determined with the enthalpy form are in that case exactly identical.

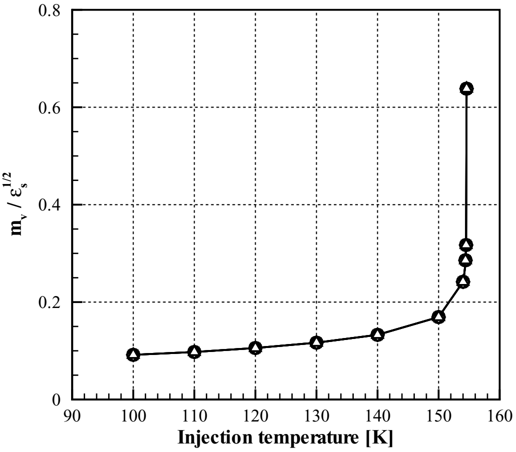

Figure 9. Evolution of the mass transfer rate divided by the square root of the strain. This quantity is plotted as a function of the injection temperature of the transcritical oxygen stream for different strain rates: 40 s^{-1} (○), 100 s^{-1} (□), 1000 s^{-1} (◇), 10 000 s^{-1} (∇). The ambient pressure is fixed at 7 MPa.

3.1. *Fundamental equations*

Using standard notations [25] and considering the special case of stationary counterflow flames the set of equations describing transcritical strained flames or transcritical counterflows established in a two-dimensional configuration may be written as follows:

$$\rho\epsilon\widehat{U} + \frac{\partial(\rho v)}{\partial z} = 0 \tag{16}$$

$$\epsilon(\rho\widehat{U}^2 - \rho_{+\infty}) + \rho v\frac{\partial\widehat{U}}{\partial z} - \frac{\partial}{\partial z}\left(\mu\frac{\partial\widehat{U}}{\partial z}\right) = 0 \tag{17}$$

$$\rho v\frac{\partial Y_k}{\partial z} + \frac{\partial}{\partial z}(\rho Y_k V_k) - \omega_k W_k = 0\,, \qquad (k = 1, ..., N) \tag{18}$$

$$\rho v\frac{\partial h}{\partial z} - \frac{\partial}{\partial z}\left(\lambda\frac{\partial T}{\partial z}\right) + \frac{\partial}{\partial z}\left(\sum_{k=1}^{N}\rho Y_k h_k V_k\right) = 0 \tag{19}$$

where ϵ is the imposed strain rate, $\rho_{+\infty}$ is the density at $z = +\infty$, and h the total enthalpy. This set is complemented by the equation of state (1), the mixture thermodynamic functions and transport algorithms and coefficients. One also has to specify transport algorithms for heat and species diffusion. It is known from non-equilibrium thermodynamics that species diffusion is due to concentration and temperature (Soret effect) gradients and that correspondingly heat diffusion is driven by temperature and species (Dufour effect) gradients. The cross-diffusion phenomena are present in perfect gases and in real gases as well [26]. These cross-diffusion terms are discussed for example by Harstad and Bellan [27]. It is generally admitted that the Dufour effect is essentially negligible as shown for example in [10, 28, 29] so that the total heat flux vector is nearly identical to the standard Fourier expression.

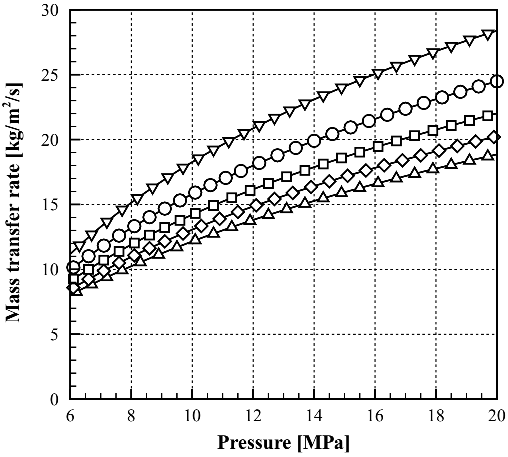

Figure 10. Evolution of the mass transfer rate with the pressure for different injection temperatures of the transcritical oxygen stream: 140 K (∇), 130 K (○),120 K (□), 110 K (◇), 100 K (△). The strain rate is fixed at 10 000 s^{-1}.

The impact of the Soret effect on the mass flux is estimated in some previous studies. Curtis and Farrell [26] indicate that the Soret and Dufour effects are significant in real fluids particularly when large ratios of the molecular weights of pure compounds are present. Direct numerical simulations of non-premixed flames [29] indicate that the Soret effect modifies the maximum flame temperature and the flame thickness. This effect is most important when one of the main species is hydrogen. The Soret effect is included by Ribert *et al.* [10] in their calculation of oxygen/hydrogen strained flames under high pressure conditions. As expected, a flux of light molecules takes place towards the hot gases while the heavier species diffuse in the opposite direction. However, the cross-diffusion terms are found to have a moderate impact on the flame structure.

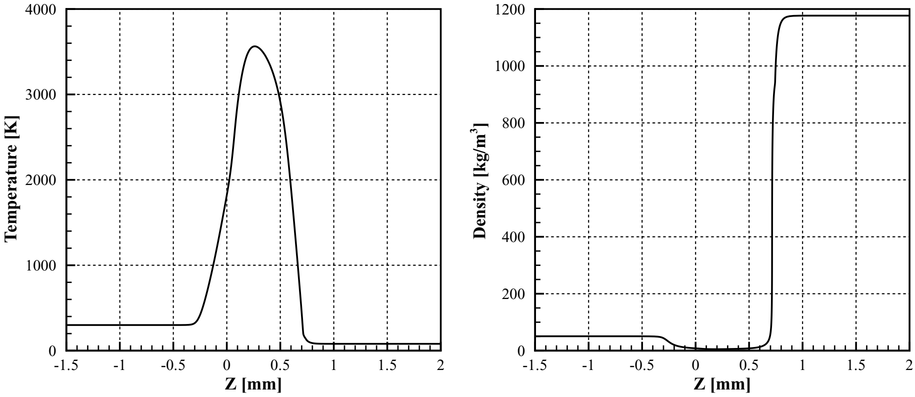

(a) Temperature profile (b) Density profile

Figure 11. Temperature and density profiles in a counterflow non-premixed flame formed by transcritical oxygen stream injected at 80 K impinging on a supercritical methane stream injected at 300 K. The ambient pressure is fixed at 7 MPa and the strain rate at $\epsilon_s = 20$ s^{-1}.

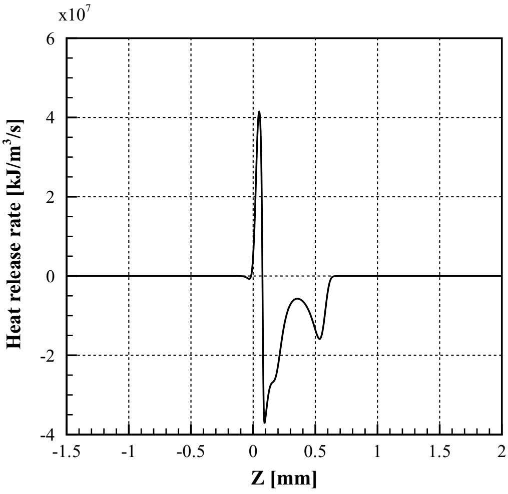

Figure 12. Heat release rate profile in a counterflow non-premixed flame formed by transcritical oxygen stream injected at 80 K impinging on a supercritical methane stream injected at 300 K. The ambient pressure is fixed at 7 MPa and the strain rate at $\epsilon_s = 20\ \mathrm{s}^{-1}$.

The present calculations are carried out for oxygen/methane flames where these cross-diffusion should be weaker and they are not taken in consideration in the present investigation to focus on the essential effects related to the very large changes in density and the effects of pressure and temperature on transport coefficients.

3.2. *Numerical details*

Calculations carried out in this study correspond to counterflow non reactive configurations and to non-premixed strained laminar flames formed by pure oxygen impinging on pure methane. The set of equations given in Equations (16)–(19) pertains to an imposed strain rate formulation. Numerical technique is discussed in [24]. The computational domain size is 10 mm and is dynamically rescaled and a new mesh is generated to accommodate strong gradients and fast changes in these gradients. The reaction mechanism, taken from [30, 31] features 29 species and 141 reactions. Real gas thermodynamics and transport are obtained from the TransChem library discussed previously while complex chemistry is handled with Chemkin package [21].

In the case of the non-reacting opposed flow (Problem 1), transcritical oxygen is injected at $z = +\infty$ at a temperature T_{inj} varying between 100 K and the critical temperature, T_{c}. Supercritical oxygen is injected at $z = -\infty$ at $T_{\mathrm{amb}} = 1000$ K. The ambient pressure is kept constant at 7 MPa.

In the cases of reacting flow, oxygen is injected at $z = +\infty$ at 80 K while methane is injected at $z = -\infty$ at 300 K (Problem 2) or 120 K (Problem 3).

4. Results of calculations

Three main calculation cases are considered in this article: (Problem 1) Non-reacting opposed flow formed by injecting a transcritical stream of oxygen against a supercritical stream of the same species; (Problem 2) Non-premixed strained laminar flame of transcritical oxygen flowing against gaseous methane; (Problem 3) Flame formed by a stream of

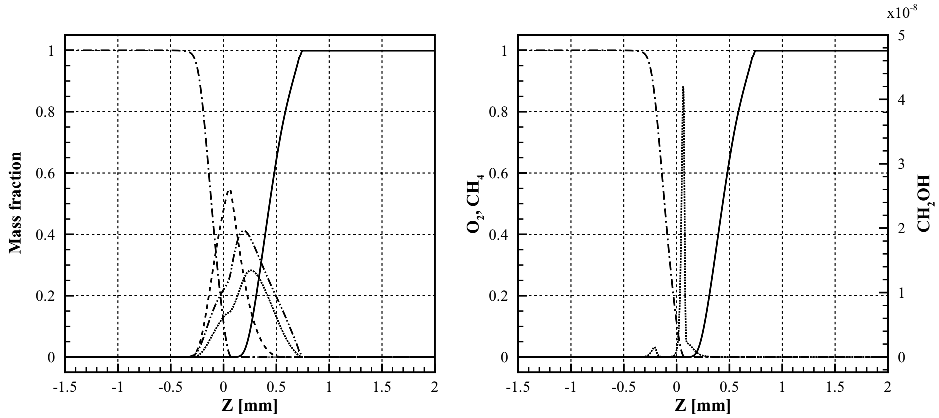

(a) Major species profiles (solid: O_2,– - – : CH_4, - - : CO_2,– – : CO, – - - – : H_2O)

(b) Minor species profiles (- - : CH_2OH)

Figure 13. Major and minor species profiles in a counterflow non-premixed flame formed by transcritical oxygen stream injected at 80 K impinging on a supercritical methane stream injected at 300 K. The ambient pressure is fixed at 7 MPa and the strain rate at $\epsilon_s = 20$ s^{-1}.

transcritical oxygen impinging on a stream of transcritical methane. These three cases are considered successively.

4.1. *Counterflow of transcritical and supercritical oxygen*

The configuration considered in this first case can be used to model the injection process in high performance liquid-rocket engines. In these systems one of the reactants is injected at a temperature below critical while the ambient pressure is above the critical value, and the environment is at high temperature. The transcritical dense jet of oxygen is surrounded by higher temperature oxygen of much lower density. When heated, this reactant passes continuously from a dense, low-temperature state, to a light, high-temperature one. During

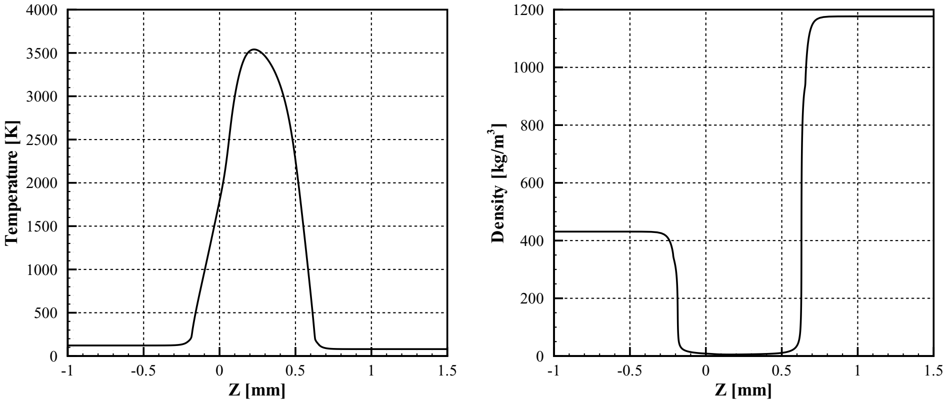

(a) Temperature profile

(b) Density profile

Figure 14. Temperature and density profiles in a counterflow non-premixed flame formed by transcritical oxygen stream injected at 80 K impinging on a transcritical methane stream injected at 120 K. The ambient pressure is fixed at 7 MPa and the strain rate at $\epsilon_s = 20$ s^{-1}.

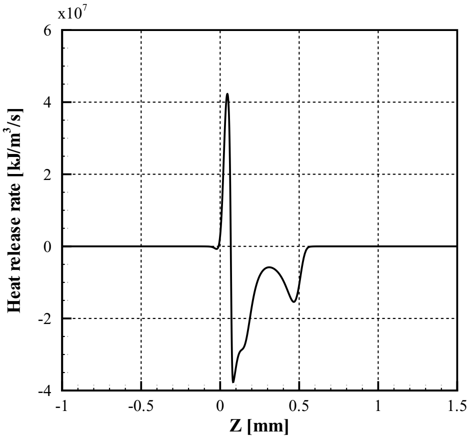

Figure 15. Heat release rate profile in a counterflow non-premixed flame formed by transcritical oxygen stream injected at 80 K impinging on a transcritical methane stream injected at 120 K. The ambient pressure is fixed at 7 MPa and the strain rate at $\epsilon_s = 20\ \mathrm{s}^{-1}$.

this transition, there is no interface between dense and light phases but there is a region where the mass density rapidly changes as a function of temperature. This strong density gradient region is easily visualized using backlighting [32]. The first configuration considered in this subsection is studied to examine a structure including subcritical and supercritical forms of the same species and estimating the mass transfer between the dense low temperature fluid and the surrounding 'vapour'. When the ambient pressure is above critical, the mass transfer process replaces the more familiar vaporization mechanism characterizing liquid injection. This study is aimed to provide the rate at which transfer takes place under transcritical injection of oxygen. This rate is determined as a function of the major parameters influencing this process like the imposed strain rate ε, injection temperature T_{inj}, ambient temperature T_{amb} and critical temperature T_{c}. The ambient pressure is fixed at a value of 7 MPa which is approximately that used in model scale experiments by Singla *et al.* [2]. The same calculations can be repeated at higher pressures but results obtained at a single pressure are easily transposed to other pressure values. Transcritical oxygen is injected at $T_{\mathrm{inj}} < T_{\mathrm{c}}$ while the impinging supercritical oxygen jet is injected at 1000 K. The kinetic scheme is reduced to one species giving the same species oxygen according to a single step fictitious reaction.

Figures 5(a) and 5(b) respectively display profiles of temperature and density as a function of the axial coordinate z. The profiles correspond to different injection temperatures of the transcritical oxygen stream from 100 K to 154.581 K which is exactly equal to the critical value. A strong density gradient is formed in this case in relation with the rapid change of density with temperature which characterizes transcritical fluids. The gradient reaches values of about $2\ 10^6\ \mathrm{kg{\cdot}m^{-4}}$. The density evolves from a liquid-like value in the transcritical region to a gaseous-like density in the supercritical zone. When the injection temperature of one of the streams is below critical, a small change of the injection temperature produces a large variation of the injected oxygen density. The gradient is stronger as the injection temperature of the transcritical fluid is diminished. This parameter strongly affects the flow and will clearly influence the mass transfer rate from the dense zone to the light region.

Mass transfer takes place across a surface separating the dense from the light fluid. This surface is somewhat arbitrary but one may use for example the isosurface corresponding to the critical temperature itself [11]. The mass transfer rate, as it is defined in this article, then corresponds to the mass of oxygen transferred per unit area of this critical temperature isosurface and per unit time. It is important to note that this definition is only meaningful when the injection temperature is below critical ($T_{\text{inj}} < T_{\text{c}}$). Figure 6 displays the calculated mass transfer rate as a function of the injection temperature of the transcritical stream for a few selected values of the strain rate. The mass transfer rate increases with the injection temperature of the cold flow and with the strain rate. The critical temperature is a singular point in the expression of the mass transfer rate and this quantity becomes infinite as the injection temperature tends to the critical value. This is linked to the definition of this rate and also reflects the physics of the process. The transfer rate is defined as the mass of reactant per unit area and per unit time crossing the critical temperature isosurface. When the injection temperature is close to the critical value less heat is needed to bring the oxygen temperature to the critical value and the mass transferred increases. When injected at the critical value, the oxygen immediately crosses the critical isosurface and the mass transfer rate becomes infinite. From studies of the behaviour of oxygen droplets in a hot high pressure hydrogen environment Yang [7] deduces an expression for the droplet lifetime as a function of a parameter which is analogous to the Spalding transfer number. A 'Spalding-like' number may be defined as suggested in [7] by considering the ratio

$$B_T = \frac{T_{\text{amb}} - T_{\text{c}}}{T_{\text{c}} - T_{\text{inj}}} \tag{20}$$

where T_{amb} is the injection temperature of the hot flow, T_{c} is the critical temperature of oxygen and T_{inj} is the injection temperature of the transcritical flow.

This 'Spalding-like' expression reflects the critical temperature singularity found in the computations of the mass transfer rate. One may then try to express the mass transfer rate from the dense zone to the light region as a function of this 'Spalding-like' number. In the case of low pressure vaporization the mass transfer rate in a boundary layer can be expressed in terms of the Spalding transfer number, B_{sp}, defined as the ratio of thermal energy per unit mass of the main stream to the thermal energy required to inject a unit mass

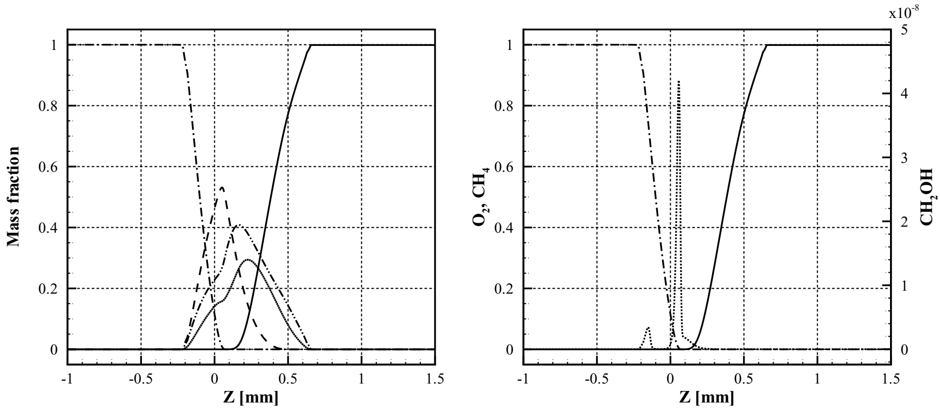

(a) Major species profiles (solid : O_2, – – – : CH_4, - -: CO_2, – – : CO, – – – – : H_2O)

(b) Minor species profiles (- - : CH_2OH)

Figure 16. Major and minor species profiles in a counterflow non-premixed flame formed by transcritical oxygen stream injected at 80 K impinging on a transcritical methane stream injected at 120 K. The ambient pressure is fixed at 7 MPa and the strain rate at $\epsilon_s = 20$ s^{-1}.

of liquid into the boundary layer:

$$\dot{m}_v = \frac{1}{2}\frac{\mu_\infty}{x}(\mathrm{Re}_x)^{1/2} f(B_{\mathrm{sp}}) \tag{21}$$

where μ_∞ is the viscosity in the free stream, x is the coordinate and Re_x is the Reynolds number based on x.

It is shown by Emmons [33] that the function f may be correctly represented by the correlation:

$$f(B_{\mathrm{sp}}) = \frac{\ln(1 + B_{\mathrm{sp}})}{1.7 B_{\mathrm{sp}}^{0.18}} \tag{22}$$

An analogy with this theory can be used to derive an expression for the mass transfer rate $\dot{m}_v$ from a transcritical stream. One considers first that $\dot{m}_v$ is a function of B_T: $\dot{m}_v \propto g(B_T)$. It is then natural to try to fit a logarithmic function $\ln(1 + B_T)$ weighted by B_T^α where alpha is an exponent to be determined. This process rapidly yields the following expression:

$$g(B_T) = \ln(1 + B_T) \tag{23}$$

where $\alpha = 0$. This correlation can be checked by plotting $\dot{m}_v/g(B_T)$ as a function of the strain rate for the different values of the oxygen injection temperature. Figure 7 indicates that the different curves collapse into a parabolic shape. It is next interesting to see how the mass transfer rate evolves with the strain rate and ambient pressure. It is known that an increase in strain rate leads to an augmented rate of transfer according to a process which has many similarities with that governing the rate of reaction in non-premixed strained flames. It is assumed for example in [11] that the mass transfer rate per unit surface area evolves like the square root of the strain rate. This issue can be examined by considering the family of curves corresponding to different values of the strain rate plotted in Figure 8 for fixed values of injection temperatures and a constant ambient pressure of 7 MPa. When the mass transfer rate is divided by $\epsilon_s^{1/2}$, all the curves collapse remarkably (Figure 9). This set of curves indicates that the mass transfer rate evolves like the square root of the strain rate as expected by analogy with gaseous strained flames [9]. It is then possible to write a general expression for the mass transfer rate which combines these various observations:

$$\dot{m}_v = 3.26\ g(B_T)\left(\frac{\varepsilon_s}{\varepsilon_{s0}}\right)^{1/2} f(p/p_0) \tag{24}$$

where $\dot{m}_v$ is given in kg m^{-2} s^{-1}, $f(p/p_0)$ a function of the pressure which equals 1 when $p = p_0$ and ϵ_{s0} and p_0 are reference strain rate and pressure (Figure 10) which have the following values: $\epsilon_{s0} = 10^4$ s^{-1} and $p_0 = 7$ MPa. The previous expression can be used in engineering estimates of the surface area required for mass transfer from a dense transcritical jet of oxygen injected in a high temperature environment.

4.2. *Strained flame formed by transcritical and supercritical streams of reactants*

In this second case a flame is produced in a counterflow by a stream of transcritical oxygen impinging on a stream of supercritical methane. Oxygen injected at $z = +\infty$ is in a transcritical state ($T_{\mathrm{LOx}} = 80$ K), with a liquid-like density of $\rho_{\mathrm{LOx}} = 1200$ kg m^{-3} whereas methane, injected at $z = -\infty$ at 300 K, has a density close to that of a gas at a pressure of 7 MPa $\rho_{\mathrm{CH4}} = 50$ kg m^{-3}. Simulations, carried out with these injection conditions, feature a temperature distribution with a maximum at the flame (Figure 11(a)) and a strong density gradient between the oxygen injection region and the flame layer as shown in Figure 11(a). This gradient is captured numerically by dynamic meshing. The rapid change in density is detected while the solution is being calculated, and the mesh is refined by shifting grid points in the gradient region. The presence of fast changes in density is highlighted in transcritical flame experiments [2] or by transcritical injection of non reactive jets [34] and it is well retrieved numerically in this admittedly simplified situation.

Figure 12 shows the profile of local heat release rate in the flame. The positive sharp peak corresponds to the methane pyrolysis region where chemical reactions are endothermic. Negative values of heat release are found on the oxygen side of the flame and correspond to the exothermic oxidation reactions taking place in this region (by convention, the heat release rate is positive when it is absorbed by the system and is negative when it is given to the environment). The flame thickness δ_f is about 0.9 mm while the reaction layer thickness $\delta_r \simeq 0.6$ mm for this relatively low level of strain rate. By comparing the heat release distribution (Figure 12) with the density profile (Figure 11(b)) one finds that the flame develops in the light-density region and that the dense oxygen acts as a nearly impermeable boundary to the flame. Main species profiles are displayed in Figure 13.

4.3. *Strained flame formed by two transcritical streams of reactants*

In the third case which is relatively non-standard, both reactants are injected under transcritical conditions. The chamber pressure of 7 MPa exceeds the critical values for oxygen ($p_c(O_2) = 5.04$ MPa) and methane $p_c(CH_4) = 4.59$ MPa), and the methane temperature is reduced to 110 K a value which is below its critical temperature $T_c = 190.564$ K. The reactant densities of methane $\rho_{\mathrm{LCH4}} = 415$ kg m^{-3} and oxygen $\rho_{\mathrm{LOx}} = 1200$ kg m^{-3} have similar orders of magnitude. The temperature profile is more symmetric than in the previous case (Figure 14). The flame thickness is also slightly reduced (Figure 15), the heat release rate profile is otherwise very similar to that obtained previously. Methans profile is also found to evolve more sharply (Figure 16). The density profile features two strong gradient layers which confine the flame. Comparing the temperature and density profiles one finds that the flame develops in the intermediate region separating the two transcritical streams and occupied by light gases. The dense streams on the two sides of the flame constitute nearly impermeable boundaries confining the reactive layer and the rate of burning is controlled by mass transfer from the two dense reactants.

5. Conclusion

This article proposes a methodology for dealing with transcritical combustion and illustrates this methodology with calculations of strained flames. Real gas effects and transport anomalies are taken into account with a library of routines designated as 'TransChem' developed to extend the more standard package Chemkin to include the high pressure, low temperature ranges corresponding to transcritical conditions. It is also shown that the balance equation of energy can be treated more conveniently in enthalpy form thus avoiding the many additional terms which must be included in the more standard temperature form. The new set of routines TransChem is then used to study generic problems involving reactants injected in a transcritical state. The study first considers the counterflow of a stream of transcritical oxygen impinging on a supercritical stream of the same species. This original model problem is used to simulate the behaviour of a dense pocket surrounded by its own vapour. The structure of this flow is calculated numerically and the mass transfer rate from the dense region is determined as a function of the strain rate. This yields a new correlation which involves a ‘Spalding-like’ transfer number. It is shown that the mass transfer rate depends on the square root of the strain rate. Supercritical methane/transcritical oxygen flames are treated as a second example. The pressure is above critical but the oxygen temperature is below critical. The flame structure features a very strong density gradient on the oxygen side of the flame (the density of oxygen drops by two orders of magnitude between the injected stream and the flame region). Reactive flow simulations are also carried out in the most unusual case where both methane and oxygen are injected in a transcritical state. The calculations feature strong density gradients which are established on the two sides of the flame and confine the reactive zone in the light region formed between the two dense streams. The rate of burning is controlled in this case by mass transfer from the transcritical regions.

Acknowledgments

This work was supported by Snecma, CNES and CNRS. A part of this work was carried out in the framework of a collaborative program with the CFD team of Cerfacs.

References

[1] M. Juniper, A. Tripathi, P. Scouflaire, J. Rolon, and S. Candel, *Structure of cryogenic flames at elevated pressures*, Proc. Combust. Inst. 28 (2000), pp. 1103–1109.

[2] G. Singla, P. Scouflaire, C. Rolon, and S. Candel, *Transcritical oxygen/transcritical or supercritical methane combustion*, Proc. Combust. Inst. 30 (2005), pp. 2921–2928.

[3] K. Harstad, R. Miller, and J. Bellan, *Efficient high-pressure state equations*, AIChE J. 43 (1997), pp. 1605–1610.

[4] R. Miller, K. Harstad, and J. Bellan, *Direct numerical simulations of supercritical fluid mixing layers applied to heptane-nitrogen*, J. Fluid Mech. 436 (2001), pp. 1–39.

[5] J. Oefelein and V. Yang, *Modeling high-pressure mixing and combustion processes in liquid rocket engines*, J. Propulsion Power 14 (1998), pp. 843–857.

[6] N. Zong, H. Meng, and V. Yang, *Cryogenic fluid injection and mixing at supercritical conditions*, paper presented at AIAA 41st Aerospace Science Meeting and Exhibit (AIAA paper 2003-0480).

[7] V. Yang, *Modeling of supercritical vaporization, mixing, and combustion processes in liquid-fueled propulsion systems*, Proc. Combust. Inst. 28 (2000), pp. 925–942.

[8] S. Som and S. Aggarwal, *A numerical investigation of methane air partially premixed flames at elevated pressures*, Combust. Sci. Technol. 179 (2007), pp. 1085–1112.

[9] L. Pons, N. Darabiha, and S. Candel, *Pressure effects on non-premixed strained flames*, Combust. Flame 152 (2008), pp. 218–229.

[10] G. Ribert, N. Zong, V. Yang, L. Pons, N. Darabiha, and S. Candel, *Counterflow diffusion flames of general fluids: oxygen/hydrogen mixtures*, Combust. Flame 154 (2008) pp. 319–330.

[11] S. Jay, F. Lacas, and S. Candel, *Combined surface density concepts for dense spray combustion*, Combust. Flame 144 (2006), pp. 558–577.

[12] R. Reid, J. Prausnitz, and T. Sherwood, *The Properties of Gas and Liquids*, 3rd edition, McGraw Hill, New York, 1977.

[13] URL http://webbook.nist.gov/chemistry/fluid

[14] A. Congiunti, C. Bruno, and E. Giacomazzi, *Supercritical combustion properties*, paper presented at AIAA 41st Aerospace Science Meeting and Exhibit (AIAA paper 2003-0478).

[15] T. Chung, M. Ajlan, L. Lee, and K. Starling, *Generalized multiparameter correlation for nonpolar and polar fluid transport properties*, Indust. Engng Chem. Res. 27 (1988), pp. 671–679.

[16] J. Ely and H. Hanley, *Prediction of transport properties 1. Viscosity of fluids and mixtures*, Indust. Engng Chem. Fund. 20 (1981), pp. 323–332.

[17] J. Ely and H. Hanley, *Prediction of transport properties .2. thermal conductivity of pure fluids and mixtures*, Indust. Engng Chem. Fund. 22 (1983), pp. 90–97.

[18] K. Harstad and J. Bellan, *High-pressure binary mass diffusion coefficients for combustion applications*, Indust. Engng Chem. Res. 43 (2004), pp. 645–654.

[19] R. Kee, G. Dixon-Lewis, J. Warnatz, M. Coltrin, and J. Miller, *A Fortran computer code package for the evaluation of gas-phase multicomponent transport properties*, Technical Report SAND86-8246, Sandia National Laboratories, 1986.

[20] S. Takahashi, *Preparation of a generalized chart for the diffusion coefficient of gases at high pressures*, J. Chem. Engng (Japan) 7 (1974), pp. 417–420.

[21] R. Kee, F. Rupley, and J. Miller, *Chemkin-2: A Fortran chemical kinetics package for the analysis of gas-phase chemical kinetics*, Technical Report SAND89-8009, Sandia National Laboratories, 1989.

[22] H. Meng and V. Yang, *A unified treatment of general fluid thermodynamics and its application to a preconditioning scheme*, J. Comput. Phys. 189 (2003), pp. 277–304.

[23] M. Smooke, I. Puri, and K. Seshadri, *A comparison between numerical calculations and experimental measurements of the structure of a counterflow diffusion flame burning diluted methane in diluted air*, Proc. Combust. Inst. 21 (1988), pp. 1783–1792.

[24] N. Darabiha, S. Candel, V. Giovangigli, and M. Smooke, *Extinction of strained premixed propane-air flames with complex chemistry*, Combust. Sci. Technol. 60 (1988), pp. 267–285.

[25] N. Darabiha and S. Candel, *The influence of the temperature on extinction and ignition limits of strained hydrogen-air diffusion flames*, Combust. Sci. Technol. 86 (1992), pp. 67–85.

[26] E. Curtis and P. Farrell, *A numerical study of high pressure droplet vaporization*, Combust. Flame 90 (1992), pp. 85–102.

[27] K. Harstad and J. Bellan, *Mixing rules for multicomponent mixture mass diffusion coefficients and thermal diffusion factors*, J. Chem. Phys. 120 (2004), pp. 5664–5673.

[28] R. Miller, *Long time mass fraction statistics in stationary compressible isotropic turbulence at supercritical pressure*, Phys. Fluids 12 (2000), pp. 2020–2032.

[29] S. Palle, C. Nolan, and R. Miller, *On molecular transport effects in real gas laminar diffusion flames at large pressure*, Phys. Fluids 17 (2005), doi 103601.

[30] P. Lindstedt, *Modeling of the chemical complexities of flames*, Proc. Combust. Inst. 27 (1998), pp. 269–285.

[31] W. Juchmann, H. Latzel, D. Shin, G. Pieter, T. Dreier, H. Volpp, R. Lindstedt, and K. Leung, *Absolute radical concentration measurements and modeling of low-pressure $CH_4/O_2/NO$ flames*, Proc. Combust. Inst. 27 (1998), pp. 469 – 476.

[32] M. Oschwald, J. Smith, R. Branam, J. Hussong, and A. Schick, *Injection of fluids into supercritical environments*, Combust. Sci. Technol. 178 (2006), pp. 49–100.

[33] H. Emmons, *The film combustion of liquid fuel*, Z. angew. Math. Mech. 36 (1956), pp. 60–71.

[34] B. Chehroudi, D. Talley, E. Coy, *Initial growth rate and visual characteristics of a round jet into a sub- to supercritical environment of relevance to rocket, gas turbine and diesel engines*, paper presented at AIAA 37th Aerospace Science Meeting and Exhibit (AIAA paper 1999-0206).

Appendices

A. Thermodynamics and transport

This appendix provides some elements on the thermodynamic and transport formulation. Further details are available in the original references.

A.1. *Thermodynamics*

When using the Peng–Robinson equation of state, the expressions of thermodynamic functions can be derived from general equations given in (11)–(13). This, combined with the equation of state given in Equation (1), yields:

$$H = pv - RT + \left(a_m - T\frac{\partial a_m}{\partial T}\right)\ln\left(\frac{v + (1-\sqrt{2})b_m}{v + (1+\sqrt{2})b_m}\right)\frac{1}{2\sqrt{2}b_m} + H^0 \tag{25}$$

where H is the molar enthalpy of the mixture, p is the pressure, v is the molar volume calculated by the classical Peng–Robinson equation of state, R is the perfect gas constant, T is the temperature, a_m and b_m are the mixture coefficients of the Peng–Ronbinson equation, and H^0 is the enthalpy at a reference state.

$$E = \left(a_m - T\frac{\partial a_m}{\partial T}\right) \ln\left(\frac{v + (1-\sqrt{2})b_m}{v + (1+\sqrt{2})b_m}\right) \frac{1}{2\sqrt{2}b_m} + E^0 \tag{26}$$

where E is the internal energy of the mixture, and E^0 is the internal energy taken at a reference state.

The molar specific heat C_p can be expressed by:

$$C_p = -T\frac{\left(\frac{\partial p}{\partial T}\right)^2_{v,n}}{\left(\frac{\partial p}{\partial v}\right)_{T,n}} - R - T\frac{\partial^2 a_m}{\partial T^2} \ln\left(\frac{v + (1-\sqrt{2})b_m}{v + (1+\sqrt{2})b_m}\right) \frac{1}{2\sqrt{2}b_m} + C_p^0 \tag{27}$$

where C_p is the specific heat of the mixture, and C_p^0 is the specific heat taken at a reference state.

The molar constant volume specific heat, C_v, expression can be derived from that of the internal energy from:

$$C_v = \left(\frac{\partial E}{\partial T}\right)_v \tag{28}$$

One needs to determine the partial enthalpies, h_i, in order to calculate the source term in the energy balance (19). The partial enthalpy of the i-th species is then given by:

$$\begin{aligned} h_i = &\left(\frac{\sum_j X_j a_{ij} - T\sum_j X_j \frac{\partial a_{ij}}{\partial T}}{\sqrt{2}b_m} - \frac{\left(a_m - T\frac{\partial a_m}{\partial T}\right) b_i}{2\sqrt{2}b_m^2}\right) \ln\left(\frac{v + (1-\sqrt{2})b_m}{v + (1+\sqrt{2})b_m}\right) \\ &+ pv_i - RT \\ &+ \left(\frac{a_m - T\frac{\partial a_m}{\partial T}}{2\sqrt{2}b_m}\right)\left(\frac{2\sqrt{2}(b_m v_i - b_i v}{(v + (1+\sqrt{2})b_m)(v + (1-\sqrt{2})b_m)}\right) + h_i^0 \end{aligned} \tag{29}$$

where X_j is the mole fraction of the j-th species, a_{ij} is the cross term of the mixture coefficient a_m and is defined in Equation (7), b_i is the b coefficient of the equation of state for the i-th species and v_i is the partial molar volume of the i-th species.

The partial molar volume can be expressed by:

$$v_i = \frac{-1}{\left(\frac{\partial p}{\partial v}\right)_{T,n}} \left(\frac{RT}{v - b_m} + \frac{RTb_i}{(v-b_m)^2} - \frac{2\sum_j X_j a_{ij}}{v^2 + 2vb_m + b_m^2} + \frac{2a_m(v - b_m)b_i}{(v^2 + 2vb_m + b_m^2)^2}\right) \tag{30}$$

A.2. *Transport*

The viscosity of high pressure fluids is suitably represented by the Chung *et al.* [15] model and is given by:

$$\eta = \eta^* \eta^0 \tag{31}$$

where η^0 is the low pressure viscosity and η^* is a correction for real gases. The low pressure viscosity is given by:

$$\eta^0 = \frac{a F_{\mathrm{cm}} \sqrt{W_m T}}{V_{\mathrm{cm}}^{2/3} \Omega_v} \tag{32}$$

where a is a constant, F_{cm} is a polar function, W_m is the molar mass of the mixture, V_{cm} is the critical volume of the mixture, and Ω_v is the collision integral.

The polar function F_{cm} depends on the acentric factor, ω_m, a correction factor for highly polar substances, k_m, and a dimensionless dipole moment, μ_{rm}.

$$F_{\mathrm{cm}} = 1 - 0.2756\omega_m + 0.053035\mu_{rm}^4 + k_m \tag{33}$$

The collision integral, Ω_v, is expressed in terms of temperature and specific coefficients by:

$$\Omega_v = A(T^*)^{-B} + C\exp(-DT^*) + E\exp(-FT^*) \tag{34}$$

where T^* is a reduced temperature defined as $T^* \propto T/T_{\mathrm{cm}}$, T_{cm} being the critical temperature of the mixture. The coefficients A, B, C, D, E and F are explicitly given in [15] or [14].

The correction term for high pressure η^* is given by:

$$\eta^* = \frac{1}{G_2} + E_6 y + \frac{\Omega_v}{F_{\mathrm{cm}}\sqrt{T^*}}\eta^{**} \tag{35}$$

where:

$$y = \frac{\rho V_{\mathrm{cm}}}{6} \tag{36}$$

$$G_2 = \frac{E_1(1-\exp(-E_4 y))/y + E_2 G_1 \exp(E_5 y) + E_3 G_1}{E_1 E_4 + E_2 + E_3} \tag{37}$$

$$G_1 = \frac{1-0.5y}{(1-y)^3} \tag{38}$$

$$\eta^{**} = E_7 y^2 G_2 \exp\left(E_8 + E_9 (T^*)^{-1} + E_{10}(T^*)^{-2}\right) \tag{39}$$

ρ is the mixture density. The parameters E_i are defined as $E_i = a_i + b_i\omega_m + c_i\mu_{rm}^4 + d_i\kappa_m$ where κ_m is the association factor and the coefficients a_i, b_i, c_i and d_i are given in [15] or [14].

The thermal conductivity of real gases is evaluated with the Ely and Hanley model [16, 17]. This model is based on the extended corresponding state theory. The thermal conductivity is represented by summing two contributions:

$$\lambda = \lambda' + \lambda'' \tag{40}$$

λ' arises from the transfer of energy from collisional or translational effects while λ'' describes the transfer of energy through the internal degrees of freedom.

It is assumed that this latter contribution is independent of the density and may be expressed as:

$$\lambda'' = \frac{f_{\text{int}}\eta^0}{W_m}\left(C_p^0 - \frac{5R}{2}\right) \tag{41}$$

where f_{int} has a constant value of 1.32, and C_p^0 is the ideal gas constant pressure specific heat.

The translational contribution, λ', is calculated via the corresponding states method:

$$\lambda' = \lambda'_f(\rho_f, T_f)F_\lambda \tag{42}$$

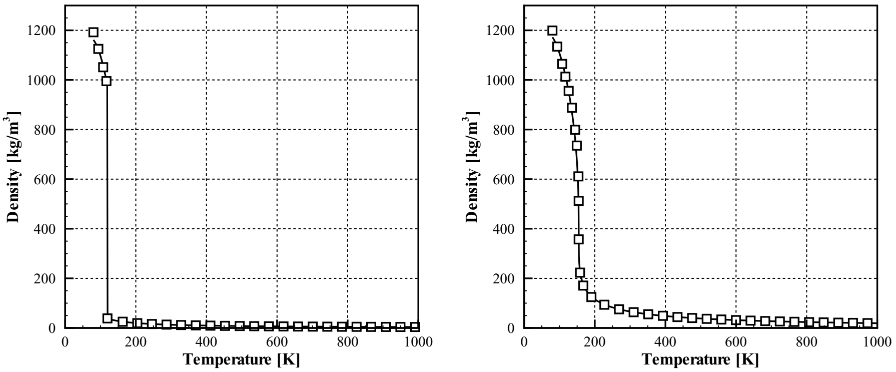

(a) p = 1 MPa (b) p = 5 MPa

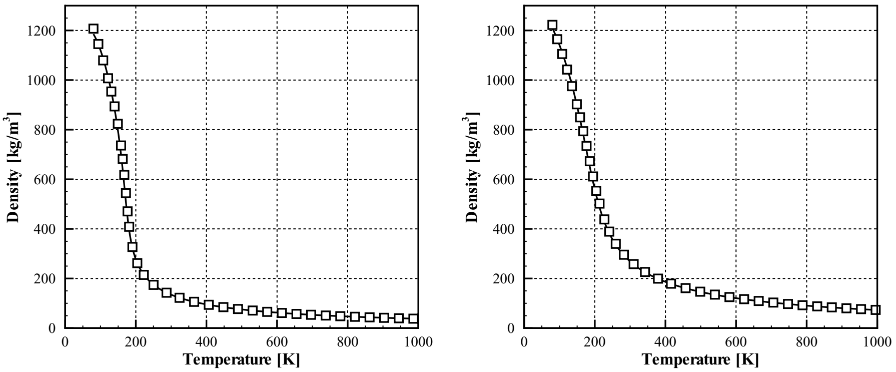

(c) p = 10 MPa (d) p = 20 MPa

Figure 17. Evolution of the density of oxygen over a range of temperatures including transcritical and supercritical states (solid: model, symbols: NIST) for different ambient pressures: (a) 1 MPa, (b) 5 MPa, (c) 10 MPa, (d) 20 MPa.

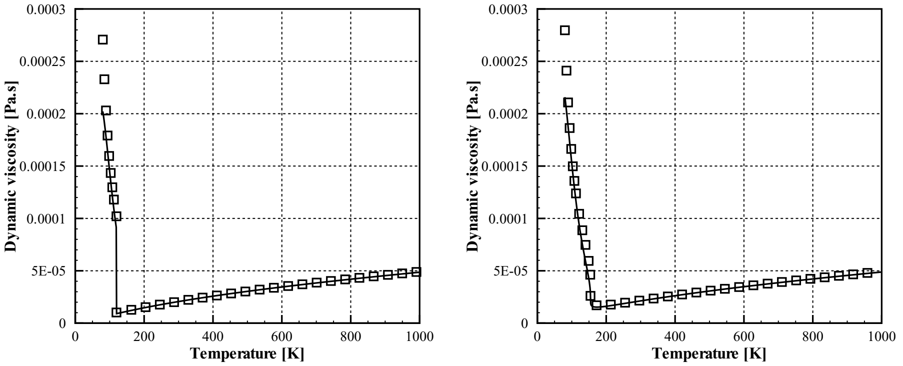

(a) $p = 1$ MPa (b) $p = 5$ MPa

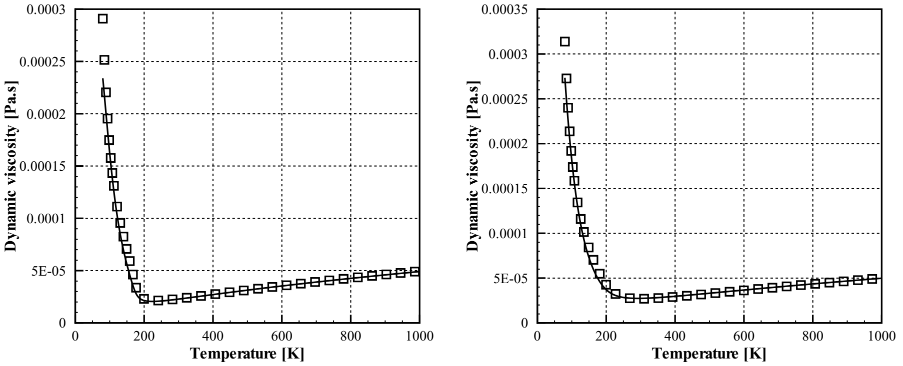

(c) $p = 10$ MPa (d) $p = 20$ MPa

Figure 18. Evolution of the dynamic viscosity of oxygen over a range of temperatures including transcritical and supercritical states (solid: model, symbols: NIST) for different ambient pressures: (a) 1 MPa, (b) 5 MPa, (c) 10 MPa, (d) 20 MPa.

The subscript f refers to the reference fluid which is methane and F_λ is given by:

$$F_\lambda = \left(\frac{W_m}{W_f}\right)^{1/2} f_{m,f}^{1/2} h_{m,f}^{-2/3} \tag{43}$$

The different terms in this last expression can be found in [16, 17].

The estimation of binary diffusion coefficients [20] is somewhat similar to the process used for viscosity. The binary diffusion coefficients are determined by the product of low pressure coefficients by the Takahashi correction.

B. Validation of the thermodynamical and transport models

Models used for the description of the thermodynamic state and transport properties of transcritical fluids are compared to reference data from the National Institute of Standards and Technology, NIST [13]. The evolution of thermodynamic functions like density, and transport coefficients like dynamic viscosity and thermal conductivity, are examined in this Appendix. Binary diffusion coefficients are not shown here because of the lack of experimental or reference data.

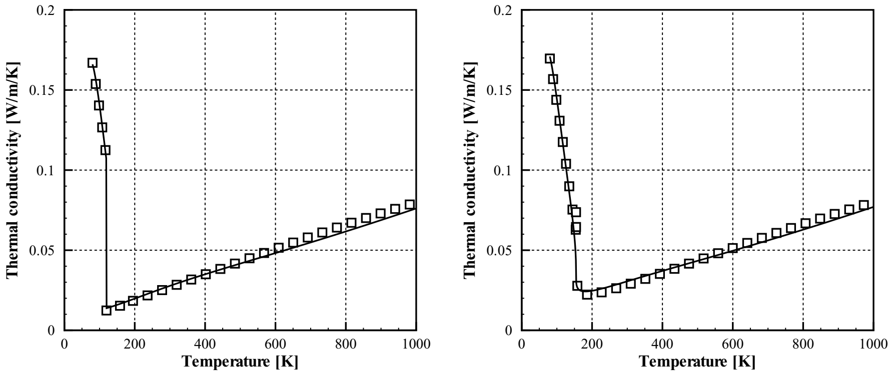

(a) $p = 1$ MPa (b) $p = 5$ MPa

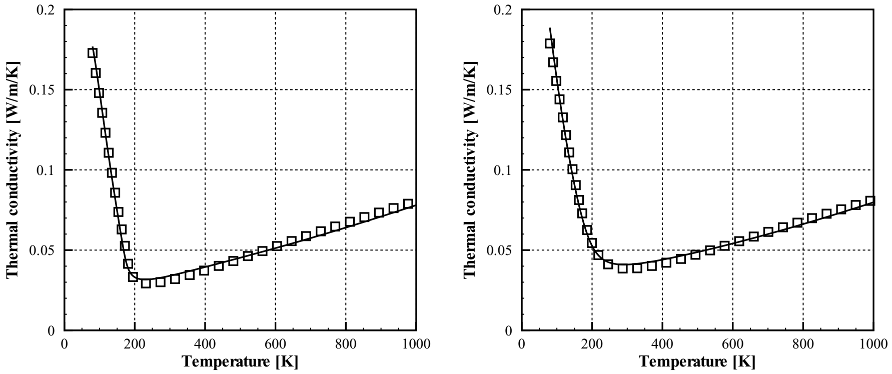

(c) $p = 10$ MPa (d) $p = 20$ MPa

Figure 19. Evolution of the thermal conductivity of oxygen over a range of temperatures including transcritical and supercritical states (solid: model, symbols: NIST) or different ambient pressures: (a) 1 MPa, (b) 5 MPa, (c) 10 MPa, (d) 20 MPa.

Figures 17, 18, 19 show the evolution of density, dynamic viscosity and thermal conductivity of oxygen under various pressures from 1 MPa to 20 MPa and for temperatures covering both the transcritical, or liquid state, and the gaseous phase (from 80 to 1000 K).

Density is accurately represented by the modified Peng–Robinson equation of state [3] whether the pressure is below or above critical. Phase transition is well located as shown in Figure 17(a). The liquid state density is slightly underestimated whatever the pressure. The near-critical region, characterized by an important density variation for a small change on temperature, is suitably described (Figure 17(b) to 17(d)). At higher temperatures, the fluid behaves like a perfect gas and is well represented by the Peng–Robinson equation of state which approaches ideal gas law at supercritical temperature.

Dynamic viscosity is given by Chung *et al.* model [15] and is compared to the NIST data in Figure 18. The viscosity in a liquid or transcritical state is underestimated for all the considered pressure, but as pressure increases, the deviation from the NIST data decreases. The phase transition is well predicted as well as the near critical region. The supercritical state is suitably described by the model.

The Ely and Hanley model [16, 17] provides suitable results for the thermal conductivity of oxygen whether the pressure is below or above critical as shown in Figure 19. The low temperature thermal conductivity is well estimated. Phase transition from liquid to gas or from transcritical to supercritical state is accurately calculated.